MECHANIKA TEORETYCZNA
I STOSOWANA
Journal of Theoretical
and Applied Mechanics
1, 34, 1996

# FORMULATION OF A BONDLINE ELEMENT FOR MODELING GLUED JOINTS IN WOOD

RICHARD M. GUTKOWSKI

*Department of Civil Engineering, Colorado State University, Ft. Collins, CO, USA*

CONRAD JAUSLIN

*Jauslin & Stebler Ing. AG., Mittenz, Switzerland*

PATRICK J. PELLICANE

*Department of Forest Sciences, Colorado State University, Ft. Collins, CO, USA*
*e-mail: patp@picea.cnr.colostate.edu*

In this study, a computer model was developed to predict the elastic stresses and strains in an articulated wood member containing a thin bondline between adherents. This model used the finite element method with an innovative bondline element to characterize the thin layer of glue between members. This element was adopted from a published model for the behavior of massive rock formations containing thin veins of different materials. Comparisons were made between numerical results obtained in this study and theoretical predictions derived from certain problems with known closed-form solutions. Very close agreement between numerical and theoretical results were found in all problems. Also, numerical predictions were compared to experimental data obtained from instrumented tests of small wood members. Once again, good agreement between numerical and experimental results was found. In addition to verification studies, parameter studies were conducted to determine the numerical stresses in step, scarf, and finger joints in wood and an isotropic material with similar stiffness.

## 1. Introduction

A recent issue of the Journal of the International Association for Bridge and Structural Engineering (see *Structural Engineering International*, 1993, **3**, 2) was devoted to new, large and innovative timber structures. The eight

bridges, sports facilities and convention centers illustrated a variety of structures which used timber in nontraditional ways. For example, the 192 meter long pedestrian bridge in Essing, Germany, with the geometry of a catenary structure, converts about 90 percent of the vertical loads into tension forces on the glue-laminated (glulam) members. This concept is unique for a timber bridge of this size. The Swiss Polydome is a 25 meter span timber shell exhibition hall with a spherical cap roof which is modelled as a stiffened shell. All ribs and decking of the shell are made with one standard small size of dimension lumber, 27 mm × 120 mm (approximately 1 × 5 in$^2$). Finally, the Hamar Olympic Indoor Stadium, built for the 1994 Winter Olympic Games, is the largest wood structure ever built. With a geometry reassembling an inverted Viking ship, the structure utilized 2 000 m$^3$ of glulam members, 40 000 dowels in the joints, and has arched trusses with spans varying between 30 and 96 meters. The designers claim that the arched truss geometry should span 130 meters without difficulty.

The previously mentioned structures became a reality due to the fact that solid lumber could be articulated into larger sizes. Glulam structural members are available due to the existence of finger jointing technology. However, with the demand for structures with greater span and load-carrying capacity, it is becoming more important that finger joint behavior under load be better understood and better predicted. In this paper, a finite element is detailed which models the glue line in articulated wood structural members. This element is incorporated into an analysis model to predict the stress and strain distributions in finger jointed wood members.

## 2. Statement of the problem

A typical vertical finger joint in a wood laminate is shown in Fig.1. A sawtooth pattern of cuts is made in adjoining pieces which are then mated by gluing. This allows the transfer of axial load across the interface in either direct tension or tension due to bending.

Although the process of making the connection is simple, the mechanical behavior of the finger joint under applied stress is complex. Because different member widths are manufactured, the cut pattern is typically unsymmetrical about the longitudinal centerline. The alternating taper cut and edge intercepts lead to stress concentrations of varying magnitude across the joint. The small clearance at each tip, made to prevent crushing of the tips, creates a stress discontinuity. In addition, wood is anisotropic and has natural variabi-

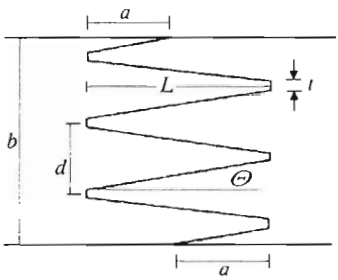


Fig. 1. Finger joint and associated nomenclature; $L$ – finger length, $b$ – laminate width, $\Theta$ – taper angle, $t$ – tip width, $d$ – tip depth, $a$ – tapered edge length

lity, as such physical properties of each piece are not identical. This is further complicated by the presence of physical defects such as knots, slope of grain, grain deviation and many other peculiarities.

Mathematical modeling of a finger joint by a closed-form solution is intractable. Consequently, numerical modeling techniques have evolved as the basis for studying the mechanical behavior of a finger joint. A number of researchers have elected to employ the finite element method (FEM) to mathematically idealize the problem. A particularly challenging aspect is the proper representation of the extremely thin glueline. However, in research to date, simplifying assumptions have been made to reduce the engineering mechanics of a glued interface to a more readily tractable problem (cf Blömer (1961); Ehlbeck et al. (1985); Leichti (1988)). An important limitation in many works has been the neglect of the glueline itself in the mesh generation (cf Qu and Fan (1988); Pellicane and Moody (1988); Pellicane (1994)). In this paper, a contact element is described whereby this limitation is overcome. The formulation of this element, as well as validation data and theoretical parameter studies, are presented herein.

## 3. Background

Only recently have researchers attempted to mathematically predict the behavior of actual finger joint geometries. Previously, a number of analytical studies had been conducted on modeling simpler geometries for glued joints in wood members.

In an early study, Goland and Reissner (1944) examined the stress distribution in a lap joint modeled as a plane-strain system. The joint they

examined is shown in Fig.2. It was treated as a plate having the dimensions $2C$ and $2T$ for its lap and width, respectively. The edge loads of this plate were obtained by considering the two bonded sheets to act as a cylindrically bent plate with a variable neutral plane passing through the points $A$ and $B$. The sheet dimensions were taken as $L + 2C$ in length and $T + n/2$ in depth, with $n$ representing the glueline thickness.

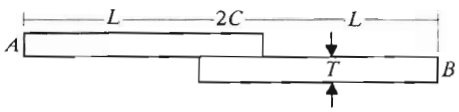


Fig. 2. Elevation view of a joint system

Two limiting cases were analyzed. In the first case, the glueline was assumed to be so thin and stiff, relative to the dimensions and stiffness of the bonded sheets, that its discontinuity could be neglected. In effect, the plate was treated as having no glueline. In the second case, the influence of the bonded sheets in the area of the overlap was neglected, and only the stress distribution in the glue was studied. Graphical results were presented. Results showed that in case 1, the peel stress concentration factor was as high as 4.3 for the loading considered. In case 2, the stress concentration was much lower. It was also observed that, compared to the shear stresses, the peel stresses were more sensitive to glueline flexibility. By decreasing the stiffness of the glueline, stress concentrations of the peel stresses could become lower than those of the shear stresses.

Erdogan and Ratwani (1971) investigated the shear stresses in the glueline of lap and scarf joints. They examined the condition of different materials on either side of the joint but neglected all bending effects. Shear stresses in the glue were highest at the edge towards the more flexible material. It was shown that the stress concentrations increase with decreasing glueline thickness.

The influence of orthotropic material properties on the stress distribution in a lap joint was analyzed by Suzuki (1990). He neglected the glueline discontinuity (Goland and Reissner (1944), first limiting case). Results showed that the stress concentrations are lowered when the stiffer material axis is parallel to the glueline. Also, the maximum peel stresses do not occur next to the glueline, but about 0.2 times the lap thickness away from it.

Using the FEM, Goodman et al. (1968) developed a "joint element", and used it to study the effect of joints and seams in massive rocks. Barker and Hatt (1973) adopted this element to analyze an adhesive joint bonding an advanced composite to a metallic adherent, and referred to it as an "adhesive

element". Schäfer (1974) used the same element, for the numerical formulation of contact problems, but called it a "bond element". Pellicane (1992) discussed the potential of the joint for modeling articulated wood members under axial load. Milner and Yeoh (1991) adopted this element to study the problem of glued finger joints in timber, but called it a "bond-line element".

Though various authors attached different names to the element, and considered it for different applications, the following common basic assumptions were made:

- The bondline is thin relative to its length
- Only normal (peel) stresses, perpendicular to the bondline, and shear stresses, parallel to the bondline, are transferred
- Both stresses are constant across the bondline.

## 4. Objective

The objective of this paper is to describe and demonstrate the validity of a computer program to predict the stress and strain distribution in finger jointed lumber exposed to uniaxial tension loading. The key component of the model which is highlighted in the paper is the finite element used to account for the thin glueline between adherents. Its formulation is also described.

## 5. Finite element analysis

The FEM is well established and has been adequately described by many authors, such as Zienkiewicz and Taylor (1989). Therefore, only a brief overview of this technique with respect to the present research is given herein.

### The FEM for linear orthotropic plane elasticity

In this study, traditional finite elements based on an approximating displacement function were used. The equilibrium equations of a continuum can be

written as

$$\begin{aligned} &\sigma_{ij,i} + f_j = 0 \qquad && P \in \Omega \\ &\sigma_{ij} n_i = t_j && P \in S \\ &\sigma_{ij} = \sigma_{ji} \end{aligned} \tag{5.1}$$

where $P$ is the point in the connected domain $\Omega$, and $S$ is the boundary of the continuum. $\sigma_{ij}$, $f_j$ and $t_j$ are the stress, body force, and the surface traction vectors, respectively, at $P$. For plane elasticity, $i, j = 1, 2$.

Eq $(5.1)_1$ is the governing equation of the stated problem, Eq $(5.1)_2$ gives the "natural" boundary conditions, and Eq $(5.1)_3$ is a consequence of the moment equilibrium at every point in the continuum.

The stress-strain relationship can be created in the form

$$\sigma_{ij} = C_{ijkl} \epsilon_{kl} \tag{5.2}$$

where $\epsilon_{kl}$ is the strain tensor at $P$, and $C_{ijkl}$ are constant material stiffnesses.

For the case of orthotropic plane elasticity, where the material axes coincide with the coordinate axes, Eq (5.2) can be written as

$$\begin{aligned} \sigma_{11} &= C_{11}\epsilon_{11} + C_{12}\epsilon_{22} \\ \sigma_{22} &= C_{21}\epsilon_{11} + C_{22}\epsilon_{22} \\ \sigma_{12} &= C_{66}\epsilon_{12} \end{aligned} \tag{5.3}$$

where

$$\begin{aligned} C_{11} &= \frac{E_1}{D} & C_{12} &= \frac{\mu_{21} E_1}{D} \\ C_{21} &= \frac{\mu_{12} E_2}{D} & C_{22} &= \frac{E_2}{D} \\ C_{66} &= G_{12} & D &= 1 - \mu_{12}\mu_{21} \end{aligned} \tag{5.4}$$

and

$E_1$ – elastic modulus (MOE) along material axis 1
$E_2$ – MOE along material axis 2
$G_{12}$ – modulus of rigidity in the 1-2 plane
$\mu_{12}, \mu_{21}$ – the Poisson's ratios.

Using energy considerations, it can be shown that $\mu_{12}/E_1 = \mu_{21}/E_2$, therefore

$$C_{12} = C_{21} \tag{5.5}$$

Hence, the stress-strain relationship can be written in the matrix form

$$\boldsymbol{\sigma}_i = \mathbf{Q}_{ij} \boldsymbol{\epsilon}_j \qquad i, j = 1, 2, 3 \tag{5.6}$$

where $\boldsymbol{\sigma}_i$ and $\boldsymbol{\epsilon}_j$ are the stress and strain vectors, respectively, at $P$ and $\mathbf{Q}_i$ is the reduced stiffness matrix.

If the material axes are rotated by an angle $\beta$, with respect to the coordinate axes, the reduced stiffness matrix $\mathbf{Q}_{ij}$ has to be pre- and post-multiplied by the 2D rotation matrices $\mathbf{T}_{ij}$ and $\mathbf{T}_{ji} = \mathbf{T}_{ij}^{\top}$, respectively. Thus, the reduced stiffness matrix $\mathbf{Q}_{ij}$ in Eq $(5.3)_2$ is replaced by rotated reduced stiffness matrix $\mathbf{Q}'_{ij}$. $\mathbf{Q}'_{ij}$ is generally a full matrix, i.e., the off-diagonal terms in the third row and third column are non-zero. For simplification, the derivations given here assume coinciding material and coordinate axes.

Assuming small deformations, the strain-displacement relationship can be written in the form

$$\epsilon_{ij} = \frac{1}{2}(u_{i,j} + u_{j,i}) \tag{5.7}$$

where $\boldsymbol{u}_i$ is the displacement vector at $P$.

Combining Eqs (5.1), (5.3) and (5.7), the equilibrium equations can be written as a function of the displacements $\boldsymbol{u}_i$ in the form

$$\begin{aligned}(C_{11}u_{1,1} + C_{12}u_{2,2})_{,1} + (C_{66}u_{1,2} + C_{66}u_{2,1})_{,2} + f_1 = 0\\ (C_{66}u_{1,2} + C_{66}u_{2,1})_{,1} + (C_{21}u_{1,1} + C_{22}u_{2,2})_{,2} + f_2 = 0\end{aligned} \tag{5.8}$$

Then, for an element with domain $\Omega_e$ and zero body forces $f_i$, the variational formulation of Eqs (5.8), can be written as

$$\begin{aligned}\int_{\Omega_e} \partial w_1 \Big[(C_{11}u_{1,1} + C_{12}u_{2,2})_{,1} + (C_{66}u_{1,2} + C_{66}u_{2,1})_{,2}\Big]\, d\Omega = 0\\ \int_{\Omega_e} \partial w_2 \Big[(C_{66}u_{1,2} + C_{66}u_{2,1})_{,1} + (C_{21}u_{1,1} + C_{22}u_{2,2})_{,2}\Big]\, d\Omega = 0\end{aligned} \tag{5.9}$$

After integrating by parts and specifying the natural boundary conditions Eq $(5.1)_2$, Eqs (5.9) can be written in the form

$$\begin{aligned}\int_{\Omega_e} \Big[(C_{11}u_{1,1} + C_{12}u_{2,2})\partial w_{1,1} + (C_{66}u_{1,2} + C_{66}u_{2,1})\partial w_{1,2}\Big]\, d\Omega = \int_{S_e} \partial w_1 t_1\, ds\\ \int_{\Omega_e} \Big[(C_{66}u_{1,2} + C_{66}u_{2,1})\partial w_{2,1} + (C_{21}u_{1,1} + C_{22}u_{2,2})\partial w_{2,2}\Big]\, d\Omega = \int_{S_e} \partial w_2 t_2\, ds\end{aligned} \tag{5.10}$$

where $S_e$ is the boundary of the element. Eqs (5.10) are often referred to as the "weak formulation" of the governing equation $(5.1)_1$.

Finally, the finite element approximation of Eqs (5.10) consists of discretizing the continuous displacement vector $\boldsymbol{u}_i$, and the continuous virtual displacement vector $\boldsymbol{w}_i$ by appropriate interpolation functions. For an isoparametric formulation, the interpolation functions for $\boldsymbol{u}_i$ and $\boldsymbol{w}_i$ are identical, i.e.

$$\begin{aligned} \boldsymbol{u}_1(x_1,x_2) &= \sum_{j=1}^{n} u_{1j}p_j(x_1,x_2) & \boldsymbol{u}_2(x_1,x_2) &= \sum_{j=1}^{n} u_{2j}p_j(x_1,x_2) \\ \boldsymbol{w}_1(x_1,x_2) &= \sum_{j=1}^{n} w_{1j}p_j(x_1,x_2) & \boldsymbol{w}_2(x_1,x_2) &= \sum_{j=1}^{n} w_{2j}p_j(x_1,x_2) \end{aligned} \tag{5.11}$$

where

$n$ – number interpolation points or number of nodes per element

$p_j$ – interpolation function for point j or the shape function of node $j$.

Hence, the finite element approximation of the equilibrium Eqs $(5.1)_1$ for an element in the continuum can be written in the matrix form

$$\begin{aligned} \mathbf{K}_{11}\mathbf{K}_{12}\boldsymbol{u}_1 &= \boldsymbol{F}_1 \\ \mathbf{K}_{21}\mathbf{K}_{22}\boldsymbol{u}_2 &= \boldsymbol{F}_2 \end{aligned} \tag{5.12}$$

where

$$\begin{aligned} K_{11ij} &= \int_{\Omega_e} (C_{11}p_{i,1}p_{j,1} + C_{33}p_{i,2}p_{j,2})\, dx_1dx_2 \\ K_{12ij} &= \int_{\Omega_e} (C_{33}p_{i,1}p_{j,1} + C_{12}p_{i,2}p_{j,2})\, dx_1dx_2 = K_{21ij} \\ K_{22ij} &= \int_{\Omega_e} (C_{33}p_{i,1}p_{j,1} + C_{22}p_{i,2}p_{j,2})\, dx_1dx_2 \\ F_1 &= \int_{\Omega_e} f_1p_i\, dx_1dx_2 + \int_{S_e} t_1p_i\, ds \\ F_2 &= \int_{\Omega_e} f_2p_i\, dx_1dx_2 + \int_{S_e} t_2p_i\, ds \end{aligned}$$

## 6. Numerical formulation of the bondline element

At each point along the bondline, local orthonormal axes $(\boldsymbol{t},\boldsymbol{n})$ are defined

with $\boldsymbol{t}$ tangent and $\boldsymbol{n}$ normal to the bondline (see Fig.3). The relative displacement between two points $A$ and $B$ in Fig.3, on opposite sides of the bondline, but geometrically at the same place, defines a set of two generalized strains. These are the peeling strain and shearing strain, which produce the integrated effects of peeling displacement $\Delta \boldsymbol{u}_n$ and shear displacement $\Delta \boldsymbol{u}_t$ given by

$$\begin{aligned} \Delta \boldsymbol{u}_n &= (u_B - u_A)\boldsymbol{n} \\ \Delta \boldsymbol{u}_t &= (u_B - u_A)\boldsymbol{t} \end{aligned} \tag{6.1}$$

These relative displacements form the kinematic basis of the element.

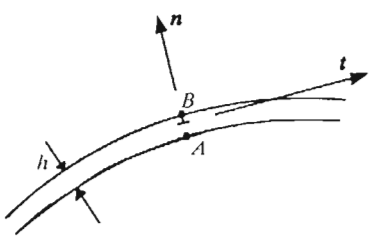


Fig. 3. Geometry and local coordinate system of a bondline element

Since the bondline elements are written for geometrically linear analysis only, the first variations of these relative displacements are identical to the above definitions, except the total values are replaced by their variations. The contribution $\partial W_e$ of one element to the virtual work is

$$\partial W_e = \int_L (\boldsymbol{F}_n \Delta \partial \boldsymbol{u}_n + \boldsymbol{F}_t \Delta \partial \boldsymbol{u}_t)\, dt \tag{6.2}$$

where

$\boldsymbol{F}_n$ – normal force per unit length of the bondline

$\boldsymbol{F}_t$ – shear force per unit length of the bondline.

The constitutive model for this element is defined as

$$\boldsymbol{F}_n = k_n \Delta \boldsymbol{u}_n \qquad \boldsymbol{F}_t = k_t \Delta \boldsymbol{u}_t \tag{6.3}$$

where $k_n = E/h$, $k_t = G/h$, and $E$, $G$ and $h$ are the moduli of elasticity and rigidity, and thickness of the bondline, respectively.

Approximating the continuous functions $\Delta \boldsymbol{u}_n$ and $\Delta \boldsymbol{u}_t$ by a finite set of nodal points along the bondline, their approximations $\Delta \boldsymbol{U}_n$ and $\Delta \boldsymbol{U}_t$ can be

written as

$$\Delta U_n(t) = \sum_{i=1}^{m}(p_i(t)\Delta U_n)$$
$$\Delta U_t(t) = \sum_{i=1}^{m}(p_i(t)\Delta U_t) \tag{6.4}$$

where interpolation polynomials $p_m(t)$ of order $m$ are employed.

Taking the virtual relative displacements $\Delta\partial\boldsymbol{u}_n$ and $\Delta\partial\boldsymbol{u}_t$ as the interpolation polynomials $p_m(t)$, and introducing Eqs (6.) and (6.4) into Eq (6.2), the finite element approximation for the virtual work contribution $\partial\boldsymbol{W}'_e$

$$\partial\boldsymbol{W}'_e = \mathbf{K}\Delta U \tag{6.5}$$

where

$$\mathbf{K} = \begin{bmatrix} \mathbf{K}_n & 0 \\ 0 & \mathbf{K}_t \end{bmatrix} \qquad \Delta U = \begin{bmatrix} \Delta U_n \\ \Delta U_t \end{bmatrix} \tag{6.6}$$

with

$$\mathbf{K}_n = \int_L \Big[\sum_{i=1}^{m} p_i(t)\frac{E}{h}p_j(t)\Big]\,dt$$
$$\mathbf{K}_t = \int_L \Big[\sum_{i=1}^{m} p_i(t)\frac{G}{h}p_j(t)\Big]\,dt \tag{6.7}$$

where $L$ is the length of the bondline.

This element has three noteworthy characteristics

1. The stiffness matrix is diagonal, i.e., $\mathbf{K}_n$ and $\mathbf{K}_t$ are uncoupled
2. Both stiffness terms are only integrated over the length $L$ of the bondline
3. The differential displacement of two coupled nodes is interpolated instead of using the first derivative of the nodal displacements.

Characteristics (1) and (2) are the mathematical formulation of the first two assumptions stated in the previous paragraph. They constitute the basis for the numerical advantage of these elements compared to normal elements. By integrating over the length, rather than over the area, the effect of the aspect ratio is removed.

Characteristic (3) can be viewed as the finite difference $(\Delta u)/h$ being computed instead of the infinitesimal rate of change $\partial u/\partial n$ across the bondline of thickness $h$. Since, according to the basic assumptions, the stresses across the bondline are constant, the expressions $\partial u/\partial n$ and $\partial u/\partial h$ are identical.

## 7. Model validity

By considering the equilibrium equations for plane elasticity with zero body forces

$$\frac{\partial \sigma_{tt}}{\partial t} + \frac{\partial \tau_{nt}}{\partial n} = 0 \qquad \frac{\partial \tau_{tn}}{\partial t} + \frac{\partial \sigma_{nn}}{\partial n} = 0 \tag{7.1}$$

some explanations regarding the three basic assumptions can be given.

According to the second assumption, the normal stresses $\sigma_{tt}$ are zero. It follows from Eq $(7.1)_1$ that the shear stresses $\sigma_{nt}$ across the bondline are constant. Consequently, the second assumption leads directly to the third one.

Because the peel stresses $\sigma_{nn}$ are constant across the bondline, Eq $(7.1)_2$ produces $\partial \tau_{tn}/\partial t = 0$. Thus, the shear stresses $\tau_{tn}$ are also constant along the bondline. However, applying moment equilibrium, yields $\tau_{tn} = \tau_{nt}$, and the conflicting observation that the shear stresses along the bondline would be constant. This observation is obviously erroneous. The first basic assumption serves to clarify this apparent contradiction. Basically, that assumption was stated that the dimension normal to the bondline can be neglected. Thus, the bondline element is a line element with a normal and a shear stiffness across the bondline, but no stiffness along the bondline. Hence, *a priori*, the equilibrium Eqs (7.1) are reduced to

$$\frac{\partial \tau_{nt}}{\partial n} = 0 \qquad \frac{\partial \sigma_{nn}}{\partial n} = 0 \tag{7.2}$$

and the mathematical basis for the contradiction is eliminated.

## 8. Finite element code

The finite element computer code developed for this work is an adaptation of software written by Thompson (1986). This modified code contains a routine (CMESH) for the mesh generation, a renumbering scheme (CNEWNUM) for the nodal points to minimize stiffness matrix bandwidth, and a standard displacement finite element code (CONTAC) for the stress-strain analysis of linear elastic solids.

CMESH originally generated a mesh for three-, four- or six-node elements of any shape composed by straight lines. The adapted code allows the inclusion of specific bondline elements with the mesh partitioned into three zones. Zone I contains all elements on one side of the bondline, Zone II elements on the other side, and Zone III consists of the elements on the bondline. The extended

mesh generator also enables the use of triangular-shaped meshes to create an orthogonal mesh pattern with a diagonal joint. This feature enables local refinement of the mesh (Fig.4).

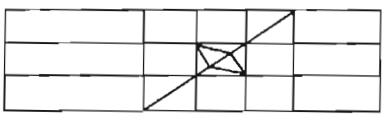

Fig. 4. Example of a scarf joint with local mesh refinement

CNEWNUM originally performed renumbering schemes for the nodal points to minimize the bandwidth of the global stiffness matrix. The adapted code accommodates elements with different numbers of nodes within the same mesh. Meshes for each of the three different zones can be renumbered separately to minimize the bandwidth of the matrices formed to find the averaged tensor stresses at each node.

CONTUAC performs the stress-strain analysis computing first the nodal displacements. The original code was extended to allow the use of different types of elements in the same analysis. CONTUAC also computes the tensor stresses within every zone. Particular routines prepare the numeric and graphic output such that the stresses and displacements of each zone and along their interfaces can be examined.

## 9. Model verification

To test the formulation and programming, analyses were performed on several problems with known solutions. Three problems considered and the outcomes were:

1. Analysis of simple butt joints between isotropic and orthotropic members under uniform axial tension produced exact results for 4-node and 6-node bond-line elements (Fig.5)

2. Erdogan and Ratwani's (1971) analytical solutions for a lap joint, were reproduced with the same accuracy as obtained by Barker and Hatt (1973) using the same bondline element (Fig.6). The discrepancy between the analytical and numerical solutions is explained by Erdogan and Ratwani's (1971) assumption of zero magnitude peel stresses

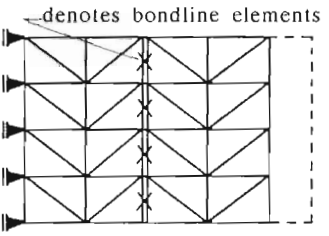


Fig. 5. Single lap joint with 32 solid triangular elements and four 4-node or 6-node bondline elements

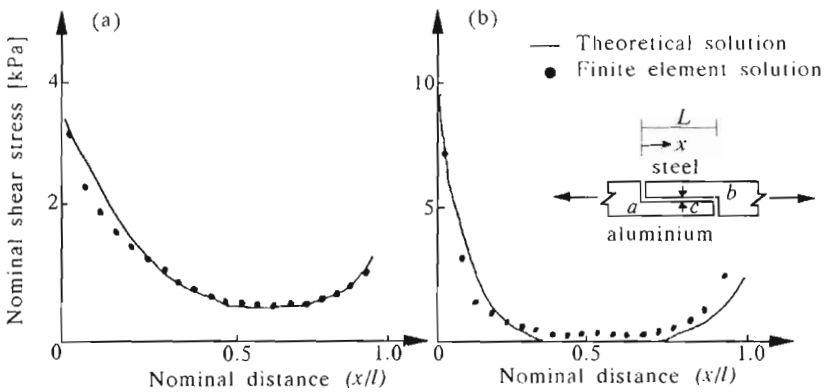


Fig. 6. Shear stress in a single lap joint, aluminum/steel; $a = b = 0.1L$, (a) – $c = 0.01L$; (b) – $c = 0.001L$

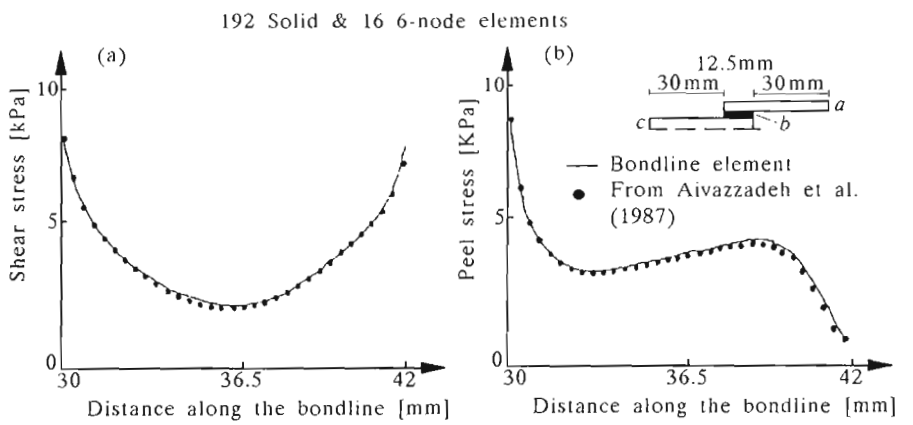


Fig. 7. Numerically-evaluated (a) shear and (b) peel stresses in the glue of a double lap joint compared to the displacement elements studied by Aivazzadeh et al. (1987); $a = 1.5$ mm, $b = 0.08$ mm, $c = 1.6$ mm

3. Near exact comparisons with the numerical solutions for a double-lap joint, reported by Aivazzadeh et al. (1987) using regular displacement finite elements, were obtained (Fig.7).

Very limited work has been reported on the subject of accurate measurement of whole-strain fields in the region of a finger joint in wood. In the work done for this paper, model predictions were compared to results obtained from tests conducted on an instrumented finger jointed wood member (cf Jauslin (1992); Pellicane et al. (1994)). Briefly, a specimen of 254 mm long, 10.7 mm wide and 2.8 mm thick with a finger jointed connection at mid-length was carefully prepared from a sample of material, tested, and monitored under repeated uniaxial tensile loadings. The preparation and instrumentation of the specimen and determination of material properties is described in the project report (Pellicane et al. (1995)).

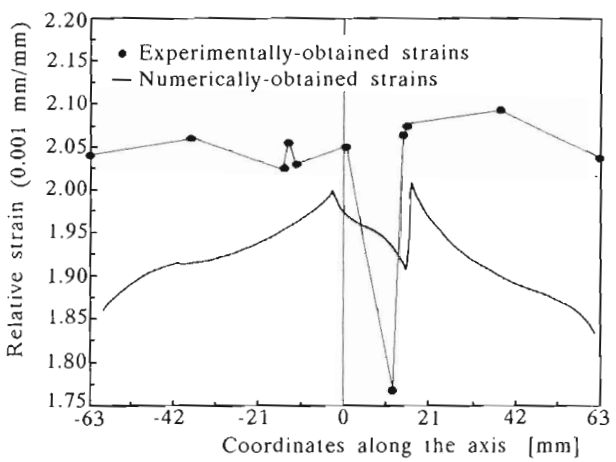


Fig. 8. Plot of experimentally- and numerically-obtained normalized displacements in a finger joint

In one experiment, high resolution photography was used to measure displacement under uniaxial tensile load between various target points along the specimen. Normalized relative displacements (at the 3.34 kN load level) along three longitudinal axes were determined from the film negatives, weighted and statistically analyzed. Resolution proved to be inadequate to trace the small variations of deformations that occurred in the specimen to accurately confirm the model. The discontinuity of the deformations at the fingertips could be observed as a general trend. This is suggested in Fig.8 which compares the weighted average of the normalized displacements for the three axes

with the predicted pattern obtained from the computer model. Unfortunately, the bandwidth of the possible error was 0.6 thousandths, which exceeds the magnitude of the apparent discontinuity.

In a second experiment, microstrain sensors (Micro-Gage Inc. (1979a,b); Pellicane et al. (1995)) were mounted along three longitudinal axes under a load of 2.22 kN, the ratio of the computed and measured strains was calculated at four sensor locations. The results showed that the strains predicted numerically matched those obtained numerically to within 18 percent on average. This is an excellent result considering the magnitude of the expected relative displacements was in the order of 2.5$\mu$m. The sensitivity of the method was evidently high enough to record variations in the strain field of the finger joint. The amount of data was limited due to the high cost of micro- strain gages and the time element of mounting these minute devices. The active length of the sensor is (1.27 mm) and its width is (0.36 mm). These ultra-thin silicon strips with a 0.038 mm diameter and electrical leads of 99.9% pure gold required about 5 hours each to mount.

## 10. Convergence of the solution

Convergence behavior of solid displacement elements, complete mixed elements and hybrid elements was examined by Aivazzadeh et al. (1987) in studies on a double-lap joint. They found that the displacement elements used were not able to curve down to zero shear stresses after the peaks close to the edges of the joint. However, the hybrid elements used did properly converge to zero at the same locations.

The authors solved the same test problem using the bondline elements for increasing fine meshes in the area of the bondline. The results showed that for the linear (4-node elements) and the quadratic (6-node elements) cases, the solution converged to the same values as for the solid displacement elements studied by Aivazzadeh et al.(1987) (Fig.7). As with the solid displacement element, the bondline element (being a particular displacement element) was unable to predict zero shear stress at the edges of the double-lap joint.

## 11. Sensitivity study of the finger joint

The prediction of finger joint behavior under uniaxial tension is an impor-

tant application for the element developed in this paper. Finger joint tensile strength is principally affected by joint geometry, wood and adhesive material properties, manufacturing procedures, and bondline mechanical and physical properties. It is not possible to study the parameters in each class independently from each other. Therefore, analyses were performed to examine extreme cases on the important variables.

## 12. Geometries and materials examined

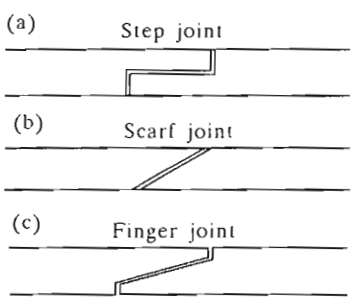


Fig. 9. Step, scarf, and finger joint geometries considered in the sensitivity study

The three geometries shown in Fig.9. Geometry (a) is referred to as a step joint, geometry (b) as a scarf joint, and geometry (c) as a finger joint. By restraining the top and bottom edges of these joints against displacement perpendicular to the longitudinal axis, geometry (c) represents the symmetric half of a complete finger joint. Hence, the finger joint can be looked at as a geometry that is between the extremes of a "step joint" and a "scarf joint". Stated differently, the step joint is the limit case of a finger joint with zero angle of taper, and the scarf joint is the limit case of a finger joint with no tip width.

Various material property conditions were investigated. The chosen material properties were:

isotropic material condition 1: $E = 13.8\,\mathrm{GPa},\ \mu = 0.3$
isotropic material condition 2: $E = 138\,\mathrm{GPa},\ \mu = 0.3$

orthotropic material condition 1: $E$ (parallel to grain) $= E_L = 15.2\,\mathrm{GPa}$
$E$ (perpendicular to grain) $= E_T =$
$= 0.69\,\mathrm{GPa}$
$G_{LT} = 0.69\,\mathrm{GPa}$, $\mu = 0.42$

orthotropic material condition 2: $E_L = 151.7\,\mathrm{GPa}$,
$E_T = 0.69\,\mathrm{GPa}$,
$G_{LT} = 0.69\,\mathrm{GPa}$, $\mu = 0.42$

adhesive: $E = 3.1\,\mathrm{GPa}$, $G = 1\,\mathrm{GPa}$

Properties for orthotropic condition 1 are those of test specimen used in the experimental phase of this study (cf Jauslin (1992); Pellicane et al. (1995)). The only difference between conditions 1 and 2 (isotropic and orthotropic) is that the value of $E_L$ is magnified tenfold. This unrealistic value for wood was used to examine effects of extreme changes. For the material properties of the glue, the values chosen were those from Erdogan and Ratwani (1971). Bondline thicknesses of 0.01 and 0.001 times the joint length, denoted $0.01L$ and $0.001L$, respectively, were used arbitrarily.

For the sensitivity study, five analytical cases were studied for all joint geometries. Isotropic cases 1 and 2 had both adherents composed of isotropic material 1 and 2, respectively. Orthotropic case 1 had both adherents composed of orthotropic material 1. Isotropic case 3 had the left and right adherents composed of isotropic materials 1 and 2, respectively. Orthotropic case 2 had the left and right adherents composed of orthotropic materials 1 and 2, respectively.

## 13. Analytical results and observations

Normal stresses parallel and perpendicular to the specimen longitudinal axis and shear stresses in the adherents on either side of the glueline were investigated. Peel and shear stresses in the glueline were also examined. These were studied for all three geometries. For clarity, Fig.10 illustrates the type of stresses examined in subsequent figures.

Extensive graphical results for the above stresses have been reported and published (cf Jauslin (1992); Jauslin et al. (1995)). Selected graphical results are shown in this paper. Fig.11 and Fig.12 are for the step joint, while Fig.13 and Fig.14 represent the scarf joint. Fig.15 and Fig.16 are for the finger joint. These graphs contain analytical results for the isotropic case 1 and orthotropic case 1 material conditions for a glueline thickness of $0.001L$. The solid and

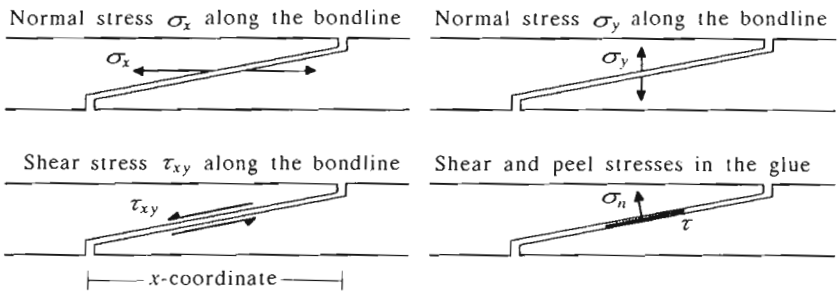


Fig. 10. Illustration of the relevant stresses considered

broken lines in the graphs refer to the stresses in the left and right adherents, respectively. Where the stresses in the glue are plotted, the solid line represents the shear stresses and the broken line the peel stresses. The principal findings demonstrated in these figures are given below.

## 14. Characteristics of all the joints studied

Some results that relate to all three types of joints are noteworthy.

- All stresses, whether normal or shear, show their peak values towards the edges of the joint. For the step joint and finger joint geometries, the peak stresses are significantly higher than the average (nominal) value. In the case of the scarf joint, stress concentrations are small in the isotropic case and essentially nonexistent in the orthotropic case. This fact emphasizes the influence of joint geometry on the stress concentrations.

- Orthotropic adherents having the strong material axis parallel to the applied tensile force show lower shear and peel stresses in the adherents near the glueline than with isotropic adherents. However, the normal stresses $\sigma_x$ parallel to the glueline are higher for orthotropic adherents than for isotropic ones.

- The shear and peel stresses in the glue joining two orthotropic adherents are higher than in the case of isotropic adherents.

- The plots for the stresses in the left and right adherents are near mirror images for each other in all cases shown.

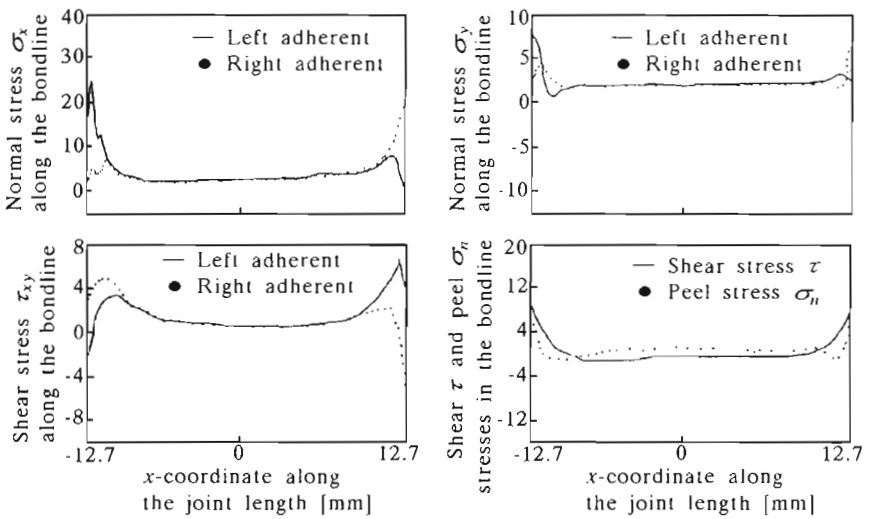


Fig. 11. Step joint/isotropic/case 1/bondline thickness = 0.001 times joint length

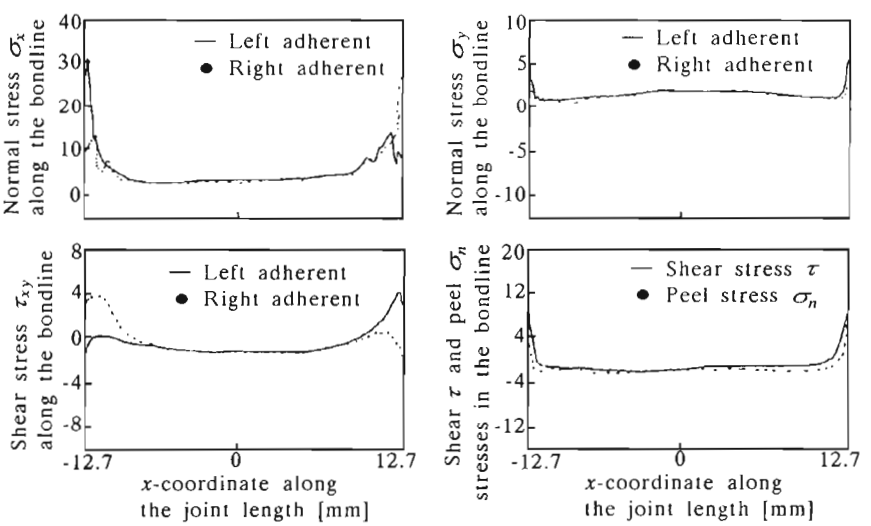


Fig. 12. Step joint/orthotropic/case 1/bondline thickness = 0.001 times joint length

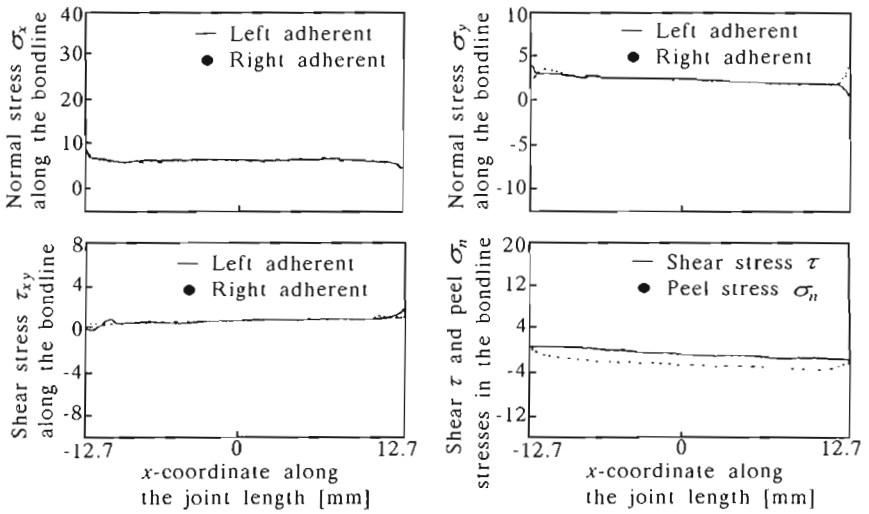


Fig. 13. Scarf joint/isotropic/case 1/bondline thickness = 0.001 times joint length

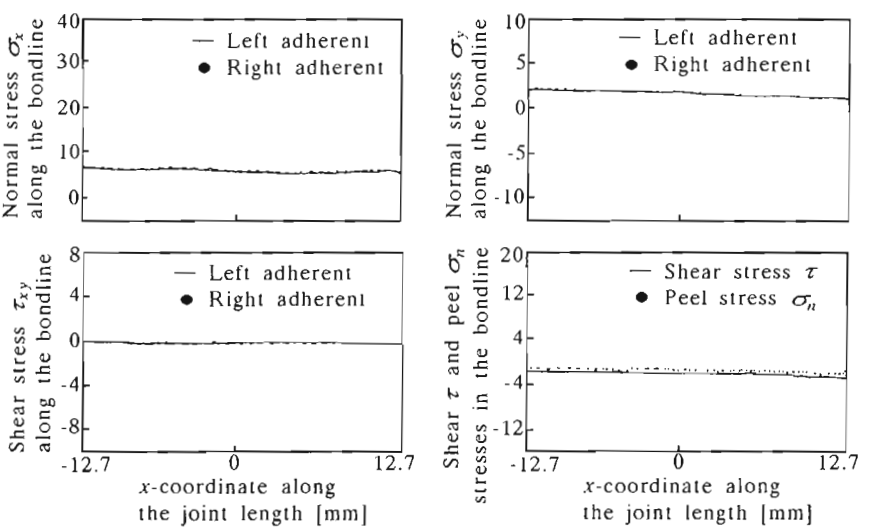


Fig. 14. Scarf joint/orthotropic/case 1/bondline thickness = 0.001 times joint length

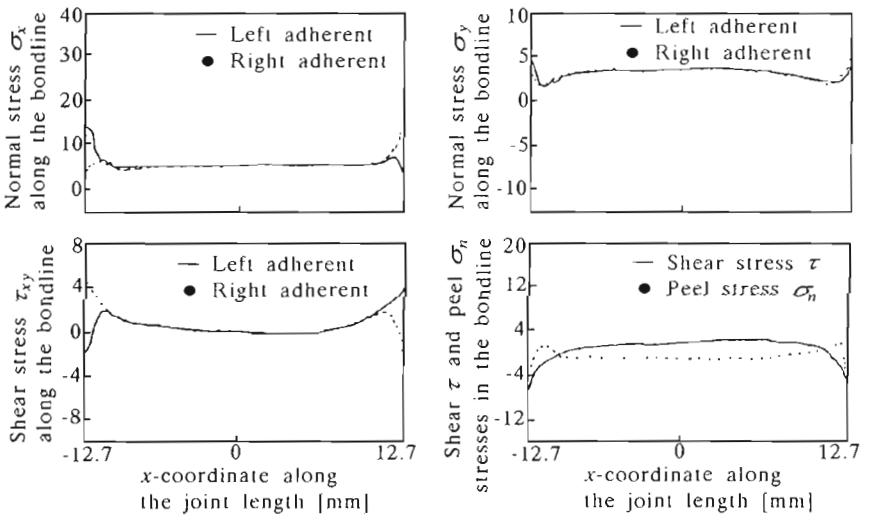


Fig. 15. Finger joint/isotropic/case 1/bondline thickness = 0.001 times joint length

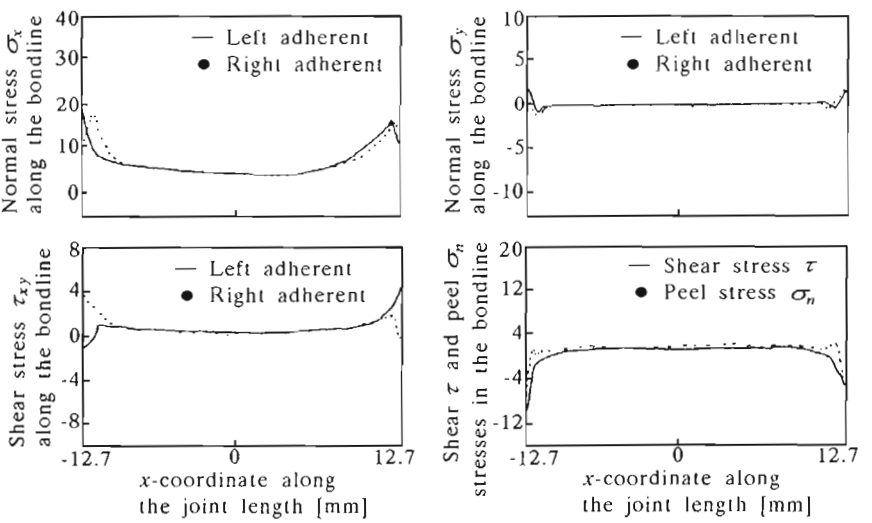


Fig. 16. Finger joint/orthotropic/case 1/bondline thickness = 0.001 times joint length

- In the interior, the adherent stresses are nearly uniformly distributed for the isotropic case 1 and are independent of geometry. Specifically, for the all joint geometries, $\sigma_x = 20.1\,\text{kPa}$, $\sigma_y = 16.5\,\text{kPa}$, $\tau = 0\,\text{kPa}$. The interior shear and peel stresses in the glueline are also essentially uniformly distributed. The interior glueline shear stress is zero for all geometries, and the interior peel stress is $13.8\,\text{kPa}$, $-13.8\,\text{kPa}$, $-13.8\,\text{kPa}$ (step, finger and scarf joint, respectively). Except for the normal stress $\sigma_y$ these levels do not noticeably change for the orthotropic case 1. The interior non-zero normal stresses for the isotropic case 1 drop to zero magnitude for the orthotropic case 1 in all joint geometries. Also, the direction of peak glueline shear and peel stresses are reversed for the step joint versus finger joint geometry.

### 14.1. Peak stresses

Wood is a material that is brittle in a tensile stress or shear stress mode, particularly for perpendicular to grain tensile stress. Thus, peak levels of these stresses are critical values to establish. From the selective results shown in this paper, it is clear that the scarf joint produces nearly uniform stresses along the glueline, for all the plotted stresses, Fig.13 and Fig.14. In contrast, significant peak stresses occur for the step joint (Fig.11 and Fig.12) and finger joint (Fig.15 and Fig.16), albeit less so for the latter configuration.

### 14.2. Step joint

Results plotted for the step joint, (Fig.11 and Fig.12), show the peak value of $\sigma_x$ is increased significantly by changing from the isotropic to the orthotropic material state. Specifically, $\sigma_x$ changes from about $0.155\,\text{MPa}$ to $0.193\,\text{MPa}$. In contrast, the peak value of $\sigma_y$ decreases, changing from about $51.7\,\text{kPa}$ to $34.5\,\text{kPa}$. The peak value of $\tau$ also decreases, changing form about $34.5\,\text{kPa}$ to $22.1\,\text{kPa}$.

### 14.3. Finger joint

Results plotted for the finger joint, (Fig.15 and Fig.16), show the peak value of $\sigma_x$ is increased slightly by changing from the isotropic to the orthotropic

material state. Specifically, $\sigma_x$ at one end of the joint changes from about 82.7 to 89.6 kPa. At the opposite end $\sigma_x$ increases much more dramatically, changing from about 48.3 to 96.5 kPa, the latter becoming the peak stress. In contrast, at one end of the joint, $\sigma_y$ decreases from about 31.0 kPa to 11.7 kPa. At this end, the peak value of also decreases from about 27.6 kPa to 20.7 kPa. At the opposite end is essentially halved also. The peak shear and peel stresses in the glueline are apparently unaffected by the change of material state, but the interior peel stresses change from zero to about $-13.8$ kPa.

### 14.4. Scarf joint

For the scarf joint, peak stresses are not of concern in the selected graphs shown (Fig.13 and Fig.14), being either nonexistent or very small compared to the overall stress distribution. For other hypothetical conditions, this is not true and is discussed subsequently.

## 15. Stress concentrations for extreme conditions

As stated earlier, five different analytical cases with various combinations of adherents were examined. Considering all the analytical results (Jauslin (1992)), the following observations about stress concentrations were evident.

Peak stresses are generally converted to normalized values using a "stress concentration factor". In this study, the stress concentration factor for normal stresses is defined as the ratio of the maximum normal stress divided by the stress computed by dividing the tension force by the width of the specimen. The stress concentration factor for the shear stresses is defined as the ratio of the maximum shear stress divided by the stress computed by dividing the tension force by the projection of the joint length along the joint longitudinal axes.

### 15.1. Step joint

For the step joint geometry, the maximum stress concentration factors and their variations due to changes in the material stiffnesses for the different stresses are reported in Table 1. Based on the complete set of results (Jauslin (1992)) for the material conditions examined, it is evident that the primary

cause for stress concentrations is the geometry itself. Changes in material properties, in the adherents as well as in the glue, have a minor influence on the maximum stresses in the adherents.

**Table 1.** Concentration factors and maximum variation of the stresses analyzed in the step joint

| Stress | Concentration factors | | Variation | |
|---|---|---|---|---|
| [kPa] | Isotropic | Orthotropic | Isotropic | Orthotropic |
| $\sigma_x$ | 33.8 | 44.8 | 2.8 | 6.2 |
| $\tau_{xy}$ | 35.2 | 22.7 | 15.2 | 6.9 |
| $\sigma_y$ | 11.0 | 6.2 | 1.4 | 0.7 |
| $\tau$ | 128.9 | 127.6 | 103.4 | 84.1 |
| $\sigma_n$ | 13.1 | 15.2 | 10.3 | 10.3 |

### 15.2. Scarf joint

For the scarf joint geometry, a distinction must be made on the basis of the material composition of the two joined adherents. When the material properties of the adherents are the same, changes in stress concentrations and distributions are very small with respect to the material properties of the adherents or the glueline. However, the scarf joint is very sensitive to differences in the material properties from one adherent to the other.

**Table 2.** Concentration factors and maximum variation of the stresses analyzed in the scarf joint

| Stress | Concentration factors | | Variation | |
|---|---|---|---|---|
| [kPa] | Isotropic | Orthotropic | Isotropic | Orthotropic |
| $\sigma_x$ | 38.6 | 38.6 | 31.7 | 31.7 |
| $\tau_{xy}$ | 15.2 | 6.2 | 15.2 | 6.2 |
| $\sigma_y$ | 4.8 | 0.7 | 2.1 | 0.7 |
| $\tau$ | 36.5 | 37.2 | 31.0 | 29.6 |
| $\sigma_n$ | 4.1 | 4.1 | 2.1 | 3.4 |

Table 2 lists the stress concentration factors and maximum variations of the stresses in the scarf joint for the collective material conditions studied. The high concentration factors in the adherents are solely due to extreme differences considered for the stiffnesses of the adjacent adherents. The high variation between the different cases investigated indicates that for equal material properties on both sides of the joint, the concentration factor is close to

one in all cases for all stresses.

The finger joint exhibits a blend of the characteristics of the step and scarf joints. Depending on the width of the fingertip, the finger joint proved to behave more like one or the other of the two extreme cases. Stress concentrations arise as soon as the tip width is assigned a non-zero value and does not gradually increase with increasing tip width.

For the case of wood such extreme differences in the material properties, as assumed above, are unrealistic. Even large differences in the stiffness between earlywood and latewood do not exceed a ratio of about three. Hence, the highest concentration factors in the scarf joint for the normal stresses parallel to the longitudinal axis would be in the order of two.

This study demonstrates that fingertip width is the dominating factor affecting the stress concentrations. As soon as there is a notch at the fingertip, the influence of the material stiffnesses plays only a secondary role. The merit of developing an economic, dependable procedure to produce intact finger joints with zero tip width is evident.

## 16. Conclusions

A finite element program has been developed to predict the stresses and strains in any isotropic or anisotropic material containing a finger joint. The bondline element showed good predictive ability in comparison with standard FEM results of lap joints.

When numerical results obtained from this program are compared to known solutions for butt-, lap- and double lap joint, the predictions are nearly identical to theoretical results. For these joints, maximum stresses in the adherents occur at the interface with the glueline. The contrary finding, by Suzuki (1990), of maximum stresses distant from the glueline must be attributed to load eccentricities due to moment in the joint he studied. The glueline stiffness depends on the ratios $E/h$ and $G/h$. Hence, doubling the glueline thickness is equivalent to halving the stiffnesses $E$ and $G$.

For constant ratios of $E_{\text{glue}}/E_{\text{adherend}}$ and $G_{\text{glue}}/G_{\text{adherend}}$, the stress distributions in a given isotropic joint are identical. Although seemingly obvious, in past literature the influences of glue and adherent stiffnesses have often been assessed as independent effects. A high ratio of glueline stiffness to adherent stiffness tends to increase the stress concentrations at the edges of all joints studied. In the adherents, this effect is relatively small, but in the glueline, the stress peaks increase drastically.

In a step joint, the horizontal glueline constitutes a finger joint of zero taper angle which is the dominating factor causing stress concentrations. In a scarf joint, a high sensitivity of the stress concentrations with respect to differences in the material properties of the two adherents occurs. However, the extreme case examined is unrealistic for solid wood members. The dominating factor for stresses concentrations in a finger joint is the notch at the fingertip. However, the stress concentrations are not as high as in the step joint.

When data obtained from tests on solid wood pieces connected by finger joints are compared to numerical solutions, the results are very reasonable for the minute displacements involved and the difficulty associated with measuring them. Therefore, it is rational to conclude, that the model discussed in this paper is a rational vehicle to predict the elastic behavior of finger jointed wood. Regardless, the model fared very well when compared with several example cases available in the literature that had been solved by non-numerical techniques.

## References

1. AIVAZZADEH S., BABI M., VERCHERY G., 1987, Assessment and Comparison of Classical, Mixed and Interface Finite Elements in Adhesive Joints, *Proceedings of the European Mechanics Colloquium 227*, Saint-Etienne, edit. G.Verchery & A.H.Gardon, Pluralis, Paris

2. ANON, 1979a, *Semiconductor Strain Sensors. Specification Sheet/Bulk Gages*, Micro Gage, Inc., El Monte, CA

3. ANON, 1979b, *Silicon Sensors Installation*, Micro Gage, Inc., El Monte, CA

4. BARKER R.M., HATT F., 1973, Analysis of Bonded Joints in Vehicular Structures, *AIAA Journal*, 11(12), 1650-1654

5. BLÖMER A., 1961, Ein beitrag zur theorie und berechnung der geleimeten berbindungen des Ingenieur-holzbaues unter besonderer berücksichtigung der gesechäftet und keilgezinkt geleimeten jolzvergindungen, *Die Bautechnik*, 38, 325-350

6. EHLBECK J., COLLING F., GÖRLACHER R., 1985, Einfluß keilgezinkter lamellen auf die biegefestigkeit von brettschichtholzträgern, Teil 2: eingangsdaten für das rechenmodell, *Holz als Roh- und Werkstuff*. 43, 369-373

7. ERDOGAN F., RATWANI M., 1971, Stress Distribution in Bonded Joints, *Journal of Composite Materials*, **5**, 378-393

8. GOLAND M., REISSNER E., 1944, The Stresses in Cemented Joints, *Journal of Applied Mechanics*, **11**, A17-A27

9. GOODMAN R.E., TAYLOR R.L., BREKKE T.L., 1968, A Model for the Mechanics of Jointed Rock, *Journal of Soil Mechanics and Foundations Division; Proceedings of the American Society of Civil Engineers.* **3**, ASCE, New York, May, 637-659

10. JAUSLIN C., 1992, Tension Behavior of Finger Joints in Wood Laminates, Ph.D. dissertation, Colorado State University, Ft. Collins, CO, 154 pp

11. JAUSLIN C., PELLICANE P.J., GUTKOWSKI R.M., 1995, Finite Element Analysis of Wood Joints, *Journal of Materials in Civil Engineering,* **7**, 1, 50-58

12. LEICHTI R.J., 1988, Structural Finger Joints under Tensile Loading Modeled with Finite Elments and Strength Theory, *Proceedings of the 1988 International Conference on Timber Engineering.* **1**, 647-653, Forest Products Research Society, Madison, WI

13. MILNER H.R., YEOH E., 1991, Finite Element Analysis of Glued Timber Finger Joints, *Journal of Structural Engineering,* **117**, 3, 755-766

14. PELLICANE P.J., 1992, A Finite Element to Model the Glueline in Articulated Wood Members, *Forest Products Journal,* **42**, 1, 50-52

15. PELLICANE P.J., 1994, Finite Element Analysis of Finger Joints in Lumber with Dissimilar Laminates, *Forest Products Journal,* **44**, 3, 17-22

16. PELLICANE P.J., GUTKOWSKI R.M., JAUSLIN C., 1994, Effect of Glueline Voids on the Tensile Strength of Finger-Jointed Wood, *Forest Products Journal,* **44**, 6, 61-64

17. PELLICANE P.J., GUTKOWSKI R.M., JAUSLIN C., 1995, Comparison of Optically and Mechanically Measured Deformations in a Finger-Jointed Wood Tension Specimen, *Journal of Testing and Evaluation, JTEVA,* **23**, 2, 136-140

18. PELLICANE P.J., MOODY R.C., 1988, Finite Element Modeling of Finger-Jointed Lumber, *Proceedings of the 1988 International Conference on Timber Engineering,* **1**, 899-907, Forest Products Research Society, Madison, WI

19. QU Z., FAN C., 1988, Tensile Strength of Glued Finger Joints in Timber Structure and Recommendation for their Series, *Proceedings of the 1988 International Conference on Timber Engineering,* **1**, 654-662, Forest Products Research Society, Madison, WI

20. SCHÄFER H., 1975, A Contribution to the Solution of Contact Problems with the Aid of Bond Elements, *Computer Methods in Applied Mechanics and Engineering,* **6**, 335-354

21. SUZUKI S.I., 1990, Stress Analysis of Cemented Orthotropic Lap Joints, *Journal of Strain Analysis,* **25**, 1, 37-41

22. ZIENKIEWICZ O.C., TAYLOR R.L., 1989, *The Finite Element Method,* **1**, McGraw-Hill Book Company, London

## Element typu "bondline" w modelowaniu drewnianych złączy klejonych

Streszczenie

W pracy pokazano model umożliwiający określenie naprężeń i odkształceń w klejonym elemencie drewnianym, posiadającym między składnikami cienką warstwę łączącą. W modelu wykorzystano metodę elementów skończonych oraz wprowadzono nowy element łączący, który reprezentuje cienką warstwę kleju między składnikami. Model ten został opracowany na podstawie spotykanego w literaturze modelu opracowanego dla formacji skalnych zawierających żyły innych pierwiastków. Przeprowadzono porównanie otrzymanych wyników numerycznych ze znanymi z literatury wynikami rozwiązań teoretycznych, otrzymując dużą zgodność. Otrzymane wyniki numeryczne zostały porównane z wynikami doświadczeń przeprowadzonych na małych elementach drewnianych, również otrzymano dużą zgodność. Oprócz weryfikacji przeprowadzono także obliczenia naprężeń w stopniowym, skośnym i palcowym złączu drewnianym oraz w złączach w materiale izotropowym o podobnej sztywności.

*Manuscript received January 30, 1995; accepted for print September 5, 1995*